



All research students must complete the details on this form before signing at the bottom. This form must then be attached by the student as a cover sheet to the 9 month, 21 month and final thesis.

Reports submitted without this form as the cover sheet will not be marked.


Student Name	CARLES MOLINS DURAN
MSc Course	AEROSPACE DYNAMICS
Title of Work	Air-vehicle modelling and simulation - ASSIGNMENT
Due Date	06/03/2017
Cranfield Supervisor	

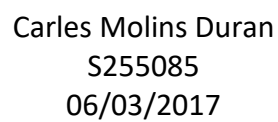
Cranfield University defines plagiarism as follows:

Plagiarism is the use, without acknowledgement, of the intellectual work of other people, and the act of representing the ideas or discoveries of others as one's own in any work submitted for assessment or presented for publication. To copy sentences, phrases or even striking expressions without acknowledgement of the source (either by inadequate citation or failure to indicate verbatim quotations) is plagiarism; to paraphrase without acknowledgement is also plagiarism.

I confirm that:

- I understand the above definition of plagiarism
- that the work contained in the attached report is all my own work except where it has been referenced accordingly
- all electronic and hard copy versions of my reports are identical
- I have given the Turnitin output summary of my report to my Supervisor(s)

Signed	
Date	06/03/2017



Index

1. Introduction	7
2. Data Dictionary	8
3. Equations of motion module	9
3.1. Construction of the equations of motion	10
3.2. Construction of the Gravity forces and moments module	11
3.3. Verification of the equations of motion	12
3.3.1. Test 1: Initial conditions	12
3.3.2. Test 2: Isolated forces	13
3.3.3. Test 3: Isolated moments	14
3.3.4. Free fall test	14
3.3.5. Pendulum test	15
4. Assembled model	16
4.1. Aerodynamic and propulsive module	17
4.2. Flight conditions module	17
5. Trim	18
5.1. Flight conditions for trim	18
5.2. Trim conditions	18
5.3. Trim results	19
5.4. Non-linear model validation with experimental data	20
5.4.1. Static validation	20
5.4.2. Dynamic validation	21
6. Lineal model	25
6.1. Construction of the lineal model	25
6.2. Validation against the non-linear model	27
7. Frequency domain analysis	30
8. Conclusions	31
8.1. Equations of motion sub-model	31
8.2. Model assembly and trim	31
8.3. Model verification	32
8.4. Linearized model and validation against the non-linear model	33
8.5. Frequency domain analysis	34
9. References	35

Index of figures

Figure 1: Photograph of the Jetstream 31.	7
Figure 2: Equations of motion subsystem flow chart.	10
Figure 3: Navigation Equations subsystem flow chart.	11
Figure 4: Implementation of the gravity forces and moments submodule with the equations of motion submodule flow chart.....	12
Figure 5: Initial conditions EoM test – lineal velocities.	12
Figure 6: Initial conditions EoM test – angular velocities.	13
Figure 7: Isolated forces EoM test results.....	13
Figure 8: Isolated moments EoM test results.	14
Figure 9: EoM free fall test.	15
Figure 10: EoM pendulum test.	15
Figure 11: Assembled model flow chart.	16
Figure 12: Flight conditions block flow chart.	18
Figure 13: Height and velocity of the simulation of the trimmed aeroplane.....	19
Figure 14: angular velocity of the simulation of the trimmed aeroplane.	20
Figure 15: Trajectory over the vertical plane of the simulation of the trimmed aeroplane.	20
Figure 16: Comparison between model simulation and experimental data- Phugoid mode.	22
Figure 17: Comparison between model simulation and experimental data- SPPO mode.	23
Figure 18: Comparison between model simulation and experimental data- Dutch roll.	23
Figure 19: Comparison between model simulation and experimental data- Roll mode.	24
Figure 20: Comparison between the non-linear and linear model – Phugoid mode.	27
Figure 21: Comparison between the non-linear and linear model – SPPO mode.....	28
Figure 22: Comparison between the non-linear and linear model – Dutch roll mode.	28
Figure 23: Comparison between the non-linear and linear model – Roll mode.	29
Figure 24: Comparison between the non-linear and linear model – Spiral mode.	29
Figure 25: Bode plot of the pitch to elevator transfer function.	30
Figure 26: Pitch attitude bandwidth requirement for flight phase category A. From MIL-STD-1797A.....	31

Index of tables

Table 1: List of all variables used for the simulation in alphabetical order.....	8
Table 2: Aeroplane loading and CG calculation.	21
Table 3: Comparison of the trim values for the inputs for the consolidated experimental data and the model.	21
Table 4: Static trim values comparison.	32
Table 5: Summary of the results of the comparison between the simulation response and the experimental data.....	33

1. Introduction

In this work the development of a non-linear simulation of a twin-engined commuter aeroplane (the Jetstream 31 (Figure 1)) has been carried out. The main tasks of this assignment have been:

- Construct a sub-model for the equations of motion and test and verify it.
- Construct a model for the aeroplane and test and verify it with experimental data.
- Generate a lineal model and contrast the results with the non-linear model.
- Carry out a frequency study to predict the handling qualities of the aeroplane.



Figure 1: Photograph of the Jetstream 31.

The basic geometric and aerodynamic parameters of the aeroplane are presented below, obtained from A. Cooke, Dynamic Stability and Modal Analysis^[1].

wing			
span	b	15.85	m
gross area	S_w	25.084	m ²
mean aerodynamic chord	\bar{c}	1.72	m
taper ratio - tip/centreline	λ_w	0.333	
lift curve slope	a_{1w}	5.122	rad ⁻¹
zero lift drag coefficient	$(C_{D0})_w$	0.007	
tail			
gross area	S_t	7.785	m ²
tail arm	l_t	6.553	m
lift curve slope	a_{1t}	3.196	rad ⁻¹
fin			
area	S_f	4.734	m ²
fin arm	l_f	6.082	m
lift curve slope	a_{1f}	2.776	rad ⁻¹
fuselage			
diameter	d	1.981	m
length	l_{fus}	13.35	m
aircraft			
mass	m	6890	kg
lift curve slope	a_1	5.764	rad ⁻¹
zero lift drag coefficient	C_{D0}	0.0376	
induced drag factor	K	0.0578	
roll inertia	I_{xx}	27300	kg.m ²
pitch inertia	I_{yy}	35765	kg.m ²
yaw inertia	I_{zz}	40080	kg.m ²

More information of the aeroplane can be found in A. Cooke, Flight Dynamic Principles: Data Pack for the Jetstream 31^[2].

2. Data Dictionary

In this section, a dictionary with all variables used for the simulation is presented in alphabetical order:

Table 1: List of all variables used for the simulation in alphabetical order.

Variable tag	Dimensions	Subvariables tag	Variable description	Units
alphaBody			Body Angle of attack	rad
Attitude	3x1 vector		Euler angles	rad
		phi	bank angle	rad
		theta	pitch angle	rad
		psi	yaw angle	rad
BetaBody			Body sideslip angle	rad
CG	3x1 vector		CG position with respect to the body axis centre	m
ETA			elevator deflection	rad
FLAP			flap position (0-Up , 1-10 deg , 2-20 deg , 3- 35 deg)	
Forces	3x1 vector		Forces expressed in the body axis	N
		X	Forces along the X-axis	N
		Y	Forces along the Y-axis	N
		Z	Forces along the Z-axis	N
INERTIA	3x3 matrix		inertia matric	kg·m2
Mach			Mach number	
MASS			mass of the aircraft	kg
Moments	3x1 vector		Moments expressed in body axis	N·m
		L	Moments along the X-axis	N·m
		M	Moments along the Y-axis	N·m
		N	Moments along the Z-axis	N·m
Omega	3x1 vector		Angular velocity given in the body axis	rad/s
		p	angular velocity along the x-body-axis	rad/s
		q	angular velocity along the y-body-axis	rad/s
		r	angular velocity along the z-body-axis	rad/s
P			Air pressure	N/m2
q			Dynamic pressure	N/m2
rho			Air density	kg/m3
T			Air temperature	K
TAU			thrust as percentage of maximum thrust	%
UC			Undercarriage position (0-Up, 1-Down)	
V			Velocity magnitude	m/s
VB	3x1 vector		Velocity given in the body axis	m/s
		u	forward velocity with respect to the body axis	m/s
		v	lateral velocity with respect to the body axis	m/s
		w	vertical (downward) velocity with respect to the body axis	m/s
VE	3x1 vector		Velocity of the airplane with respect to the earth axis [North velocity; East velocity; Downwards velocity]	m/s
Wd			Vertical acceleration expressed in body axis	m/s2

XE	3x1 vector	Position of the airplane with respect to the earth axis	m
	N	north position (position wrt earth axis)	m
	E	east position (position wrt earth axis)	m
	D	downward position (position wrt earth axis)	m
XI		aileron deflection	rad
ZETA		rudder deflection	rad

3. Equations of motion module

In this section a module to compute the equations of motion is developed (see Figure 2).

The equations of motion module gives the state of the aircraft given the forces and moments applied on it, hence its inputs are:

- Forces acting on the body expressed in body axis (Forces) in N, a 3x1 vector containing:
 - Forces along the X axis (X)
 - Forces along the Y axis (Y)
 - Forces along the Z axis (Z)
- Moments acting on the body expressed in body axis (Moments) in Nm a 3x1 vector containing:
 - Moments along the X axis (L)
 - Moments along the Y axis (M)
 - Moments along the Z axis (N)

In addition to constant data:

- Mass of the aircraft (MASS) in kg
- Inertia tensor (INERTIA), a 3x3 matrix in kg·m²
- Centre of gravity position with respect to the body axis centre (CG) in m, a 3x1 vector containing the coordinates in the x body axis, y body axis and z body axis.

And its outputs will be:

- Velocity given with respect to the body axis (VB) in m/s, which is a vector of size 3x1 containing:
 - the forward velocity with respect to the body axis (u) in m/s,
 - the lateral velocity with respect to the body axis (v) in m/s,
 - the vertical (downward) velocity with respect to the body axis (w) in m/s
- Linear acceleration with respect to the body axis (VBdot) in m/s², which is a vector of size 3x1 containing:
 - the forward acceleration with respect to the body axis (ud) in m/s²,
 - the lateral acceleration with respect to the body axis (vd) in m/s²,
 - the vertical (downward) acceleration with respect to the body axis (wd) in m/s²
- Angular velocity with respect to the body axis (Omega) in rad/s, which is a vector of size 3x1 containing:
 - The angular velocity along the x-body-axis (p) in rad/s,
 - The angular velocity along the y-body-axis (q) in rad/s,
 - The angular velocity along the z-body-axis (r) in rad/s,
- Attitude (Attitude) in rad, which is a vector of size 3x1 containing:
 - The bank angle (phi) in rad,
 - The pitch attitude (theta) in rad,
 - The yaw angle (psi) in rad
- The position with respect to local earth axis (XE) in m, which is a vector of size 3x1 containing:
 - The north position (N) in m,
 - The east position (E) in m,
 - The downwards position (D) in m.

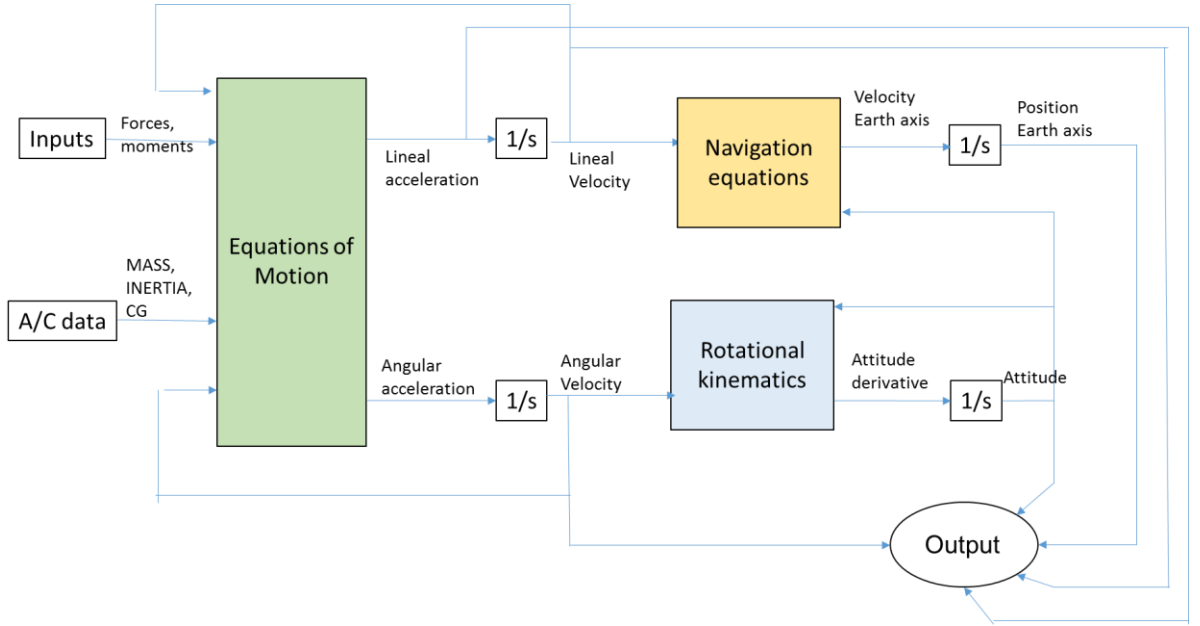


Figure 2: Equations of motion subsystem flow chart.

3.1. Construction of the equations of motion

The equations of motion module comprehends different blocks:

- **Equations_of_motion:** This first block solves the equations of motion per se. Given the forces, moments and mass properties of the aeroplane it outputs the lineal and rotational accelerations. It is set up as a matlab® function which solves the following equations:

$$\begin{bmatrix} m & 0 & 0 & 0 & md_z & -md_y \\ 0 & m & 0 & -md_z & 0 & md_x \\ 0 & 0 & m & md_y & -md_x & 0 \\ 0 & -md_z & md_y & [I_{xx}]_b & 0 & -[I_{xz}]_b \\ md_z & 0 & -md_x & 0 & [I_{yy}]_b & 0 \\ -md_y & md_x & 0 & -[I_{xz}]_b & 0 & [I_{zz}]_b \end{bmatrix} \begin{bmatrix} \dot{U} \\ \dot{V} \\ \dot{W} \\ \dot{P} \\ \dot{Q} \\ \dot{R} \end{bmatrix} = \begin{bmatrix} X + mRV - mQW + md_x(Q^2 + R^2) - md_yPQ - md_zPR \\ Y - mRU + mPW - md_xPQ + md_y(P^2 + R^2) - md_zQR \\ Z + mQU - mPV - md_xPR - md_yQR + md_z(P^2 + Q^2) \\ L - QR([I_{zz}]_b - [I_{yy}]_b) + PQ[I_{xz}]_b - (PV - QU)md_y + (RU - PW)md_z \\ M - PR([I_{xx}]_b - [I_{zz}]_b) - (P^2 - R^2)[I_{xz}]_b - (QU - PV)md_x - (QW - RV)md_z \\ N - PQ([I_{yy}]_b - [I_{xx}]_b) - QR[I_{xz}]_b - (RU - PW)md_x + (QW - RV)md_y \end{bmatrix}$$

The lineal and rotational accelerations are then integrated to obtain the lineal and angular velocities.

- **Rotational Kinematic transform:** From the angular velocity and the attitude of the aeroplane, it computes the derivative of the attitude angle (hence creating an algebraic loop). The derivative of the attitude angle is latter integrated to obtain the attitude angles themselves. The block is set up as a matlab® function which solves the equations given below:

$$\begin{bmatrix} \dot{\Phi} \\ \dot{\Theta} \\ \dot{\Psi} \end{bmatrix} = \begin{bmatrix} 1 & \sin \Phi \tan \Theta & \cos \Phi \tan \Theta \\ 0 & \cos \Phi & -\sin \Phi \\ 0 & \sin \Phi \sec \Theta & \cos \Phi \sec \Theta \end{bmatrix} \begin{bmatrix} P \\ Q \\ R \end{bmatrix}$$

- **Navigation Equations:** The navigation equations output the velocity with respect to the earth axis from the body axis velocity and the attitude of the aeroplane. It is composed of different blocks (see Figure 3):

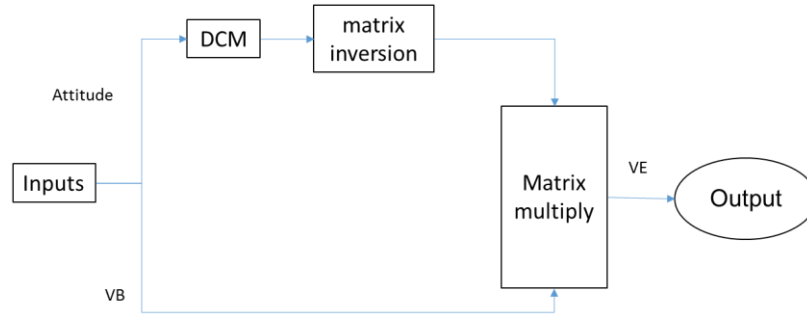


Figure 3: Navigation Equations subsystem flow chart.

The DCM_matrix block generates the Direction Cosine Matrix given the attitude. It's set up as a Matlab® function which generates the following matrix:

$$\begin{bmatrix} \cos \Theta \cos \Psi & \cos \Theta \sin \Psi & -\sin \Theta \\ -\cos \Phi \sin \Psi + \sin \Phi \sin \Theta \cos \Psi & \cos \Phi \cos \Psi + \sin \Phi \sin \Theta \sin \Psi & \sin \Phi \cos \Theta \\ \sin \Phi \sin \Psi + \cos \Phi \sin \Theta \cos \Psi & -\sin \Phi \cos \Psi + \cos \Phi \sin \Theta \sin \Psi & \cos \Phi \cos \Theta \end{bmatrix}$$

The matrix is then inverted and multiplied with the body axis velocity, which gives the local-earth axis velocity. This is later integrated to obtain the local-earth axis position. The local-earth axis position is also multiplied by a gain of [1 ; 1 ; -1] since the height component is given towards the earth centre and for visualisation it is more intuitive to have a positive height.

3.2. Construction of the Gravity forces and moments module

A module to compute the forces and moments generated by the weight of the aircraft with respect to the body axis has been developed. This module is later used as an aid to validate the Equations of Motion system, hence it is pertinent to document it here. The inputs to the module are:

- The attitude angles (Attitude)
- CG position with respect to the body axis centre in metres (CG)
- mass of the aircraft in kilograms (m)

The block as a whole is a Matlab® function that carries out the following matricial equations:

$$\begin{bmatrix} X_g \\ Y_g \\ Z_g \\ L_g \\ M_g \\ N_g \end{bmatrix} = \begin{bmatrix} 1 & 0 & 0 \\ 0 & 1 & 0 \\ 0 & 0 & 1 \\ 0 & -z_{CG} & y_{CG} \\ z_{CG} & 0 & -x_{CG} \\ -y_{CG} & x_{CG} & 0 \end{bmatrix} \cdot \begin{bmatrix} -mg \sin(\theta) \\ mg \sin(\phi) \cos(\theta) \\ mg \cos(\phi) \cos(\theta) \end{bmatrix}$$

Giving as an output two vectors:

- The force due to the weight of the aircraft expressed in body axis.
- The moments applied on the BAC due to the weight, expressed in body axis.

Its implementation with the Equations of Motion submodule is carried out as shown in Figure 4. The forces and moments calculated in this module will be summed to any other forces acting on the body (in the case of an aeroplane, the aerodynamic and propulsive forces) and input to the equations of motion module. The Equations of Motion in its turn compute the attitude angles which are input to the gravitational forces and moments module.

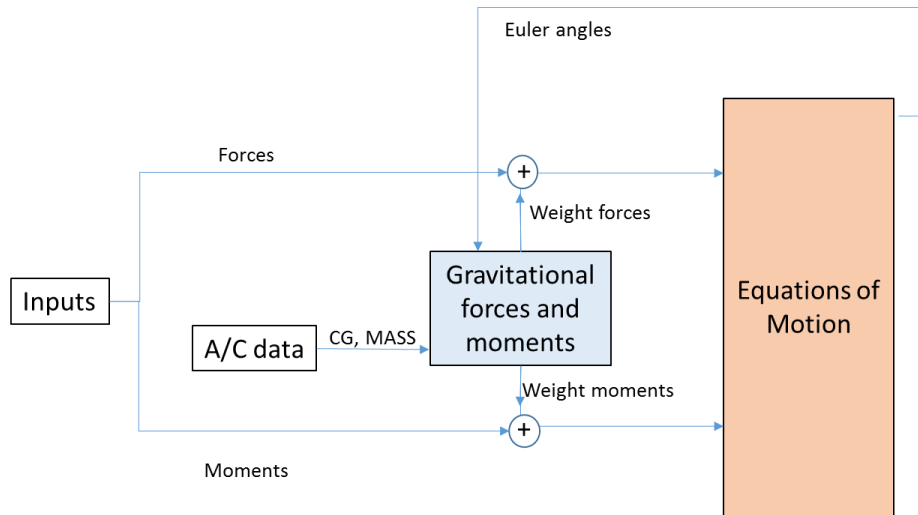


Figure 4: Implementation of the gravity forces and moments submodule with the equations of motion submodule flow chart.

3.3. Verification of the equations of motion

Five simple tests are carried out to verify the module behaviour:

- Isolated initial conditions.
- Isolated unitary forces.
- Isolated unitary moments.
- Free fall test.
- Pendulum test.

3.3.1. Test 1: Initial conditions

Firstly the lineal velocities are tested. The testing conditions are:

- Isolated initial conditions in lineal velocity.
- No forces or moments applied.

The expected result is that the body velocities remain constant. The objective of this test is to validate the fact that if no forces or moments are applied the initial conditions should remain constant.

An initial velocity condition of $V_B = [1 \ ; \ 2 \ ; \ 3] \text{ m/s}$ is used. As it can be checked in Figure 5, the velocities are maintained.

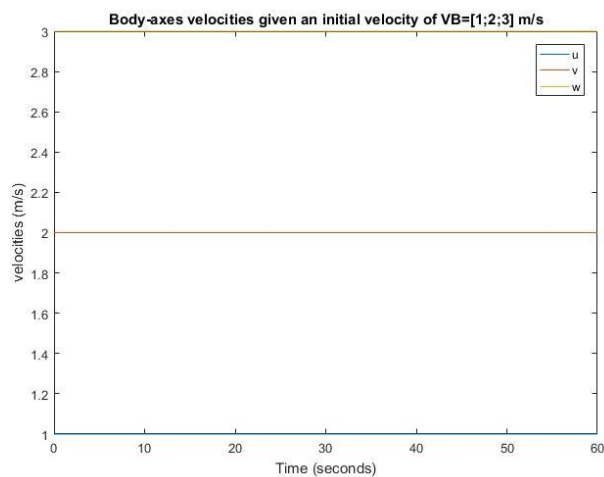


Figure 5: Initial conditions EoM test – lineal velocities.

The same is done for the angular velocities instead of lineal. An initial angular velocity condition of $\Omega=[1; 2; 3]$ rad/s is introduced. As it can be seen in Figure 6, the angular velocities are conserved.

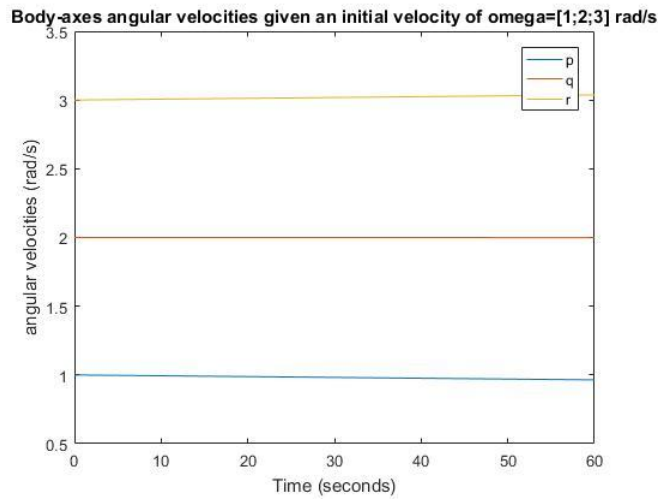


Figure 6: Initial conditions EoM test – angular velocities.

3.3.2. Test 2: Isolated forces

This test intends to ensure that there are no problems concerning the forces. The testing conditions for this test are:

- Isolated unitary forces in each direction applied at the same time.
- Initial conditions equal to zero.
- Unitary mass.

The expected result is to observe uniformly accelerated movement with a total displacement at 60 seconds of 1800m in each direction. It must be taken into account that since z is defined downwards, the z position will be negative. As it can be observed in Figure 7, the results are as expected.

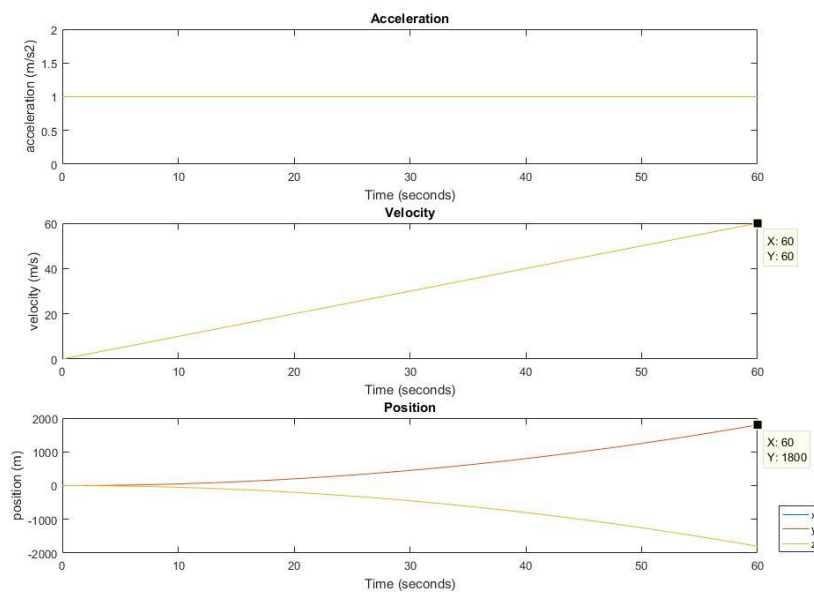


Figure 7: Isolated forces EoM test results.

3.3.3. Test 3: Isolated moments

This test intends to ensure that there are no problems concerning the moments and inertia tensor. The testing conditions for this test are:

- Isolated unitary moments over each axis applied separately.
- Initial conditions equal to zero.
- Massless body.
- Inertia tensor equal to the identity.

In this case, each moment will be applied independently to avoid coupling in the rotations. The expected result is to observe uniformly accelerated movement with a total rotation at 60 seconds of 1800rad for each direction. As it can be observed in Figure 8, the results are as expected.

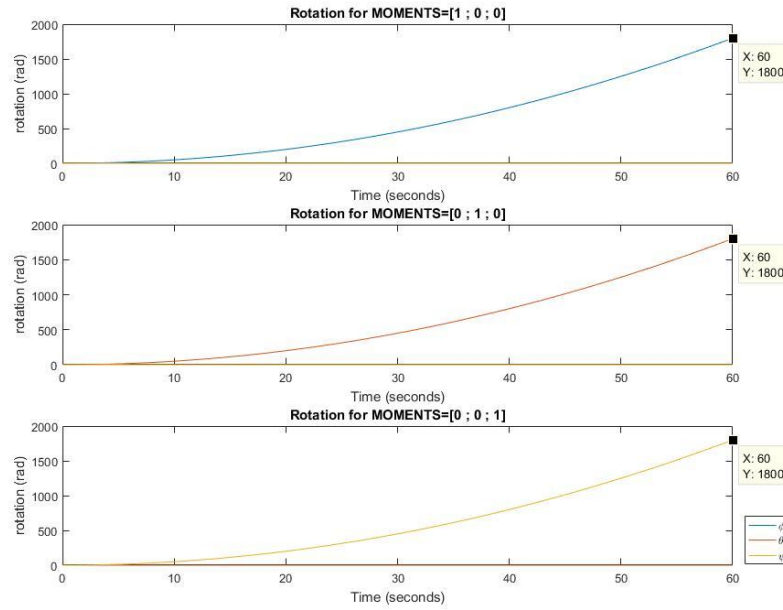


Figure 8: Isolated moments EoM test results.

3.3.4. Free fall test

For this test, the gravity forces and moments module is connected. This test intends to test both the gravitational forces and moments module as a whole and the coupling of forces and moments of the Equations of motion module. The testing conditions are:

- Forces and moments (other than the ones due to the weight) equal to zero (free fall).
- Initial altitude of 2000m.
- Initial conditions equal to zero.

The expected result is that the time to reach a height of zero is equal to that of a free fall (for 2000m fall, 20.20 seconds) and that the initial attitude does not change. As it can be seen in, the results are as expected.

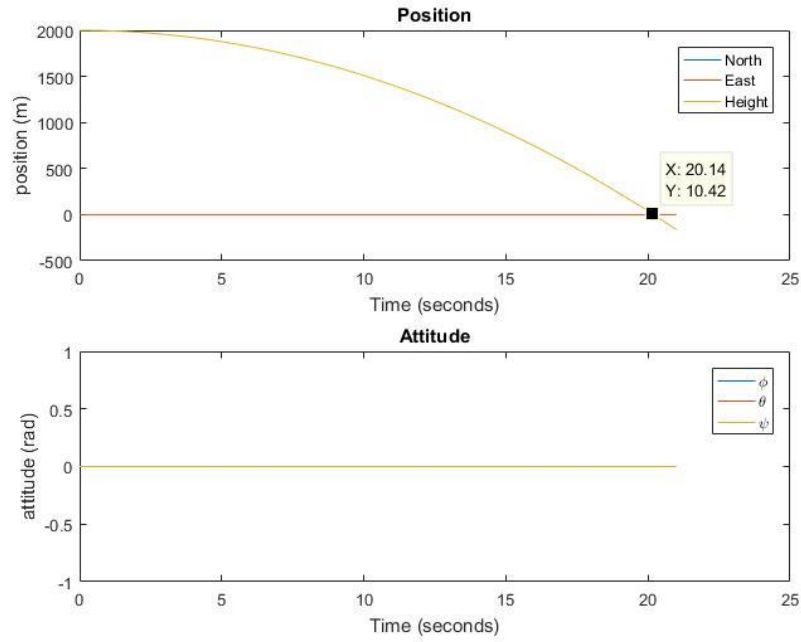


Figure 9: EoM free fall test.

3.3.5. Pendulum test

The aim of this test is to check the coupling of forces and moments of the Equations of motion module. The test conditions are as follows:

- Only the moments of the gravity forces and moments module are connected.
- Null inertia tensor.
- Initial attitude of $-\pi/4$ rad in bank angle. In pitch, the test is not carried out as the DCM matrix would go through a singular point.
- Unitary mass.
- CG position equal to $[0; 1; 0]$ m.

The response should be equal to that of a pendulum with a string of 1m oscillating from $-\pi/4$ to $-3\pi/4$ going through $-\pi$. The expected result is that the period of oscillation is equal to 2.0071 seconds. The results obtained are as expected, as seen in Figure 10.

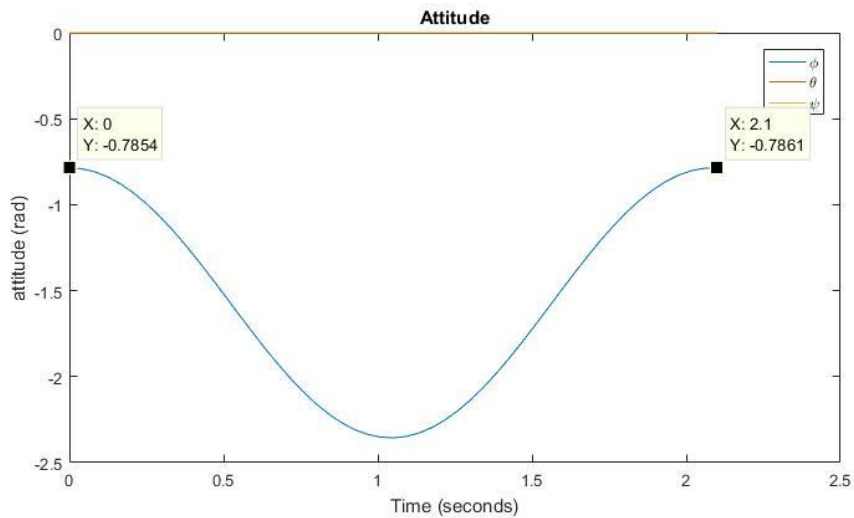


Figure 10: EoM pendulum test.

4. Assembled model

In this section the whole aircraft model is assembled. Bear in mind that for the aerodynamic and propulsive module no explanation will be given as it is not a module developed in this work.

The model consists of 4 main blocks (see Figure 11):

- the aerodynamic & propulsive module (yellow),
- the gravitational forces and moments module (blue),
- the flight conditions module (green) and
- the equations of motion module (red).

The inputs of the model are:

- The elevator deflection (ETA) in radians,
- rudder deflection (ZETA) in radians,
- aileron deflection (XI) in radians and
- thrust percentage (THAU) as a percentage of the total thrust.

Other variables input as constants are:

- CG position with respect to the body axis centre in metres (CG).
- mass of the aircraft in kilograms (MASS),
- inertia matrix in kg·m² (INERTIA),
- flap position (FLAP), which can take the values 0, 1, 2 or 3 for Up, 10 deg, 20 deg and 35 deg deflection respectively,
- undercarriage position (UC), which can take the values of 0 for retracted, 1 for deployed.

The outputs of the model are:

- velocity magnitude (V) in m/s,
- the angle of attack of the body (alphaBody) in radians and
- the sideslip angle of the body (BetaBody) in radians.

The states of the model are:

- The velocity with respect to the body axis (VB),
- The angular velocity with respect to the body axis (Ω)
- The attitude angles (Euler)
- The 'ground' position (XE).

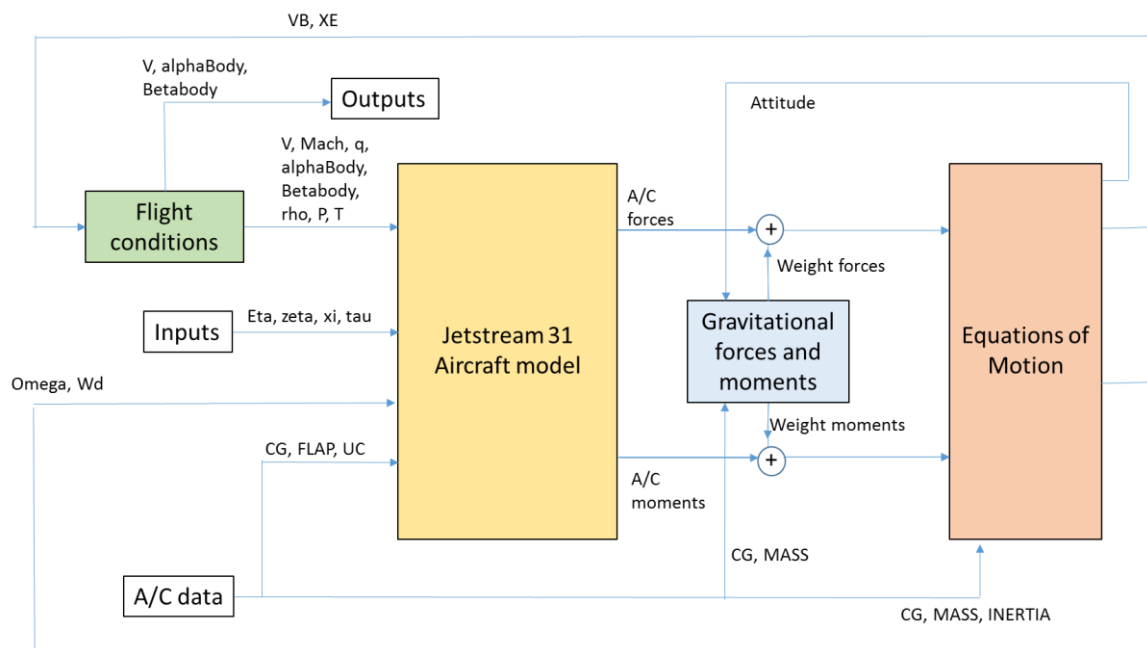


Figure 11: Assembled model flow chart.

Since the Gravitational Forces and Moments and the Equations of Motion blocks have already been explained, only the Aerodynamic and Propulsive module and the Flight Conditions module need clarification:

4.1. Aerodynamic and propulsive module

This module is treated as a black box, hence no explanation on how it works will be given. This block computes from the current state of the aircraft the forces and moments due to aerodynamic and propulsive elements about the body axis centre.

The inputs to this block are:

- The velocity magnitude (V) in m/s
- Mach number ($Mach$)
- Dynamic pressure (q) in N/m²
- Angle of attack (α_{Body}) in rad
- Sideslip angle (β_{Body}) in rad
- Air density (ρ) in Kg/m³
- Air pressure (P) in N/m²
- Air temperature (T) in K
- Angular velocity (Ω) in rad/s
- Vertical acceleration (W_d) m/s²
- Centre of gravity position with respect to the BAC (CG) in m
- Flap position ($FLAP$)
- Elevator deflection (η) in rad
- Rudder deflection (ζ) in rad
- Aileron deflection (ξ) in rad
- Thrust as a percentage of maximum thrusts (τ) in %.

These inputs will be given by the flight conditions module (V , $Mach$, q , α_{Body} , β_{Body} , ρ , P and T), the Equations of Motion module (Ω and W_d) the aircraft data (CG and $FLAP$) and the whole assembly inputs (η , ζ , ξ , τ).

The output is:

- Aerodynamic and propulsive forces along the x-axis (X), y-axis (Y) and z-axis (Z) of the body axis system in N, which is summed to the gravitational forces and fed into the Equations of Motion block.
- Aerodynamic and propulsive moments around the x-axis (L), y-axis (M) and z-axis (N) of the body axis system in Nm, which is summed to the gravitational moments and fed into the Equations of Motion block.

4.2. Flight conditions module

This module computes different flight variables from the current aeroplane velocity and flight altitude. The input for the module is:

- The velocity with respect to the body axis (VB) and
- The 'ground' position (XE)

These inputs are given by the Equations of Motion block.

The blocks diagram of the module is shown in Figure 12. From the velocity vector the body angle of attack, sideslip and the magnitude of the velocity can be computed using the Simulink® *Incidence, Sideslip & Airspeed* block. From the ground position (XE), the 3rd component (corresponding to the height of flight) is taken and fed to the Simulink® *ISA Atmosphere Model* from which the temperature (T), speed of sound (a), air pressure (P) and air density (ρ) at the given height are obtained. The velocity vector (VB) and (a) are fed to the Simulink® *Mach Number* block, which provides the Mach number ($Mach$). Finally, the velocity vector (VB) and the air density (ρ) are fed to the Simulink® *Dynamic Pressure* block, with which the dynamic pressure (q) is obtained.

The outputs of this module are:

- The velocity magnitude (V) in m/s
- Mach number
- Dynamic pressure (q) in N/m²
- Angle of attack (α_{Body}) in rad
- Sideslip angle (β_{Body}) in rad
- Air density (ρ) in Kg/m³
- Air pressure (P) in N/m²
- Air temperature (T) in K

All these outputs are fed to the Aerodynamic and Propulsive block.

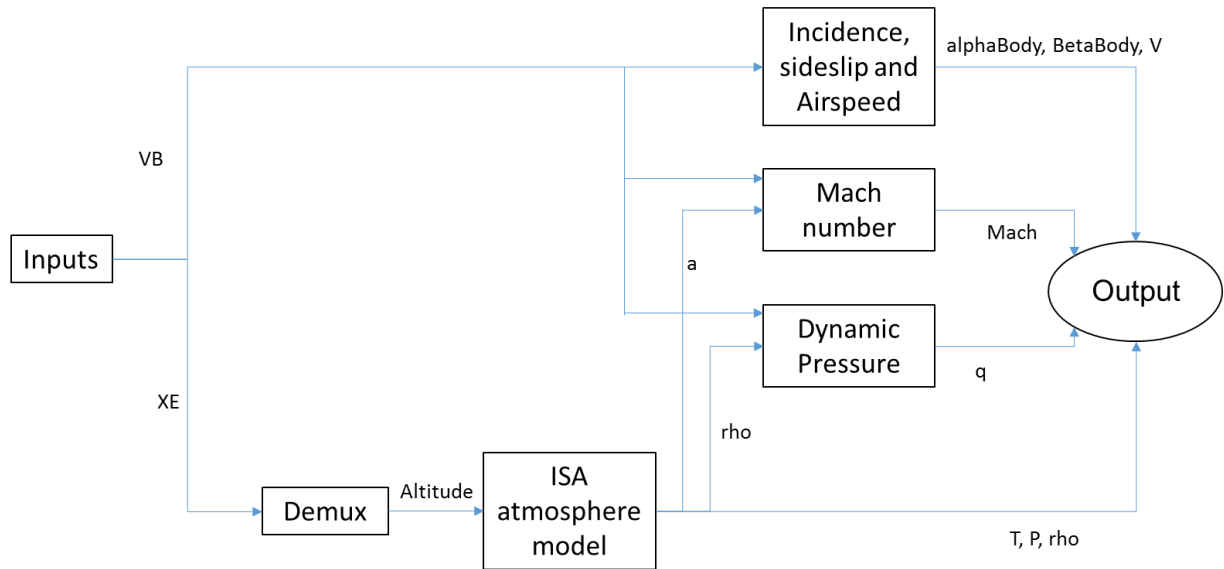


Figure 12: Flight conditions block flow chart.

5. Trim

5.1. Flight conditions for trim

The conditions chosen to trim the aircraft are the flight conditions and loading used for the test flights carried by flight group A in the second seating configuration:

- Passenger and crew loading matrix:

$$\begin{bmatrix} 86 & 0 & 69 & 65 & 64 & 86 & 0 & 180 \\ 86 & 0 & 75 & 68 & 58 & 90 & 0 & 80 \\ 0 & 0 & 75 & 69 & 50 & 120 & 0 & 0 \end{bmatrix} Kg$$
- Fuel: 656 Kg
- Flap: retracted (0)
- Undercarriage: up (0)
- Altitude: 6004 ft
- EAS: 161 kts

Setting the trim conditions to these will enable latter comparison with the experimental results.

5.2. Trim conditions

With the previous flight conditions, the variables for the trim can be initialised as follows:

- State space Variables
 - Initial velocity: [89.6 ; 0 ; 4.1] m/s
 - Initial angular velocity: [0; 0; 0] rad/s
 - Attitude: [0; 0; 0] rad;
 - Position relative to earth local axis: [0; 0; -1830] m
- Inputs:
 - Elevator deflection 0 rad.
 - Rudder deflection 0 rad.
 - Aileron deflection 0 rad.
 - Thrust 50%.
- Outputs:
 - Velocity magnitude 89.742 m/s
 - Angle of attack 0 rad
 - Sideslip angle 0 rad
- State space Variables derivatives:
 - Zero for all derivatives except for the North velocity (relative to earth local axis), which will be equal to the velocity magnitude, 89.742 m/s

The trim is carried out so that the aeroplane maintains a steady horizontal levelled flight at the given height and velocity. This means that both height and velocity need to be fixed so that the trim is done at the appropriate conditions. To ensure steady horizontal flight, all state space variable derivatives need to be fixed, and so does the angular velocities P, Q and R.

5.3. Trim results

The trim is carried out with the inbuilt matlab® function 'trim'. The results of the trim are shown below:

- State space variables:
 - $\begin{bmatrix} u \\ v \\ w \end{bmatrix} = \begin{bmatrix} 89.6 \\ 2.3 \\ 4.3 \end{bmatrix} m/s$
 - $\begin{bmatrix} p \\ q \\ r \end{bmatrix} = \begin{bmatrix} 0 \\ 0 \\ 0 \end{bmatrix} rad/s$
 - $\begin{bmatrix} \phi \\ \theta \\ \psi \end{bmatrix} = \begin{bmatrix} 0.052 \\ 0.158 \\ -0.109 \end{bmatrix} rad$
 - $\begin{bmatrix} North \\ East \\ Down \end{bmatrix} = \begin{bmatrix} 0 \\ 0 \\ -1830 \end{bmatrix} m$
- Outputs
 - $V = 89.7421 m/s$
 - $\alpha_b = 0.0476 rad$
 - $\beta_b = 0.0257 rad$
- Inputs
 - $\eta = 0.0391 rad$
 - $\zeta = 0.0595 rad$
 - $\xi = 0 rad$
 - $\tau = 51.35\%$

Now the trimmed variables can be input into the model to check if the model is really at trim. The model is simulated for 60 seconds and the modelled aeroplane should maintain a levelled flight with minimum variation in its variables.

In Figure 13 the height and velocity obtained during the simulation are shown. Since these variables define the flight condition, it is imperative that those remain as constant as possible when the model is trimmed. As it can be seen, the variation in both of them is minimal, with the maximum variation in height being a 3.35e-06% of its original value and the maximum variation in velocity a 7.17e-06% of its original value.

In Figure 14 the body angular velocities have been plotted. As it can be seen, all of them are very close to zero (being the maximum deviation -5e-06 rad/s for Q), hence it can be concluded that the aeroplane maintains its attitude along all the flight path.

Finally, in Figure 15, the vertical plane trajectory has been plotted. As it can be seen the trajectory appears to be perfectly levelled, as the variation in height is negligible compared to the distance covered towards the north.

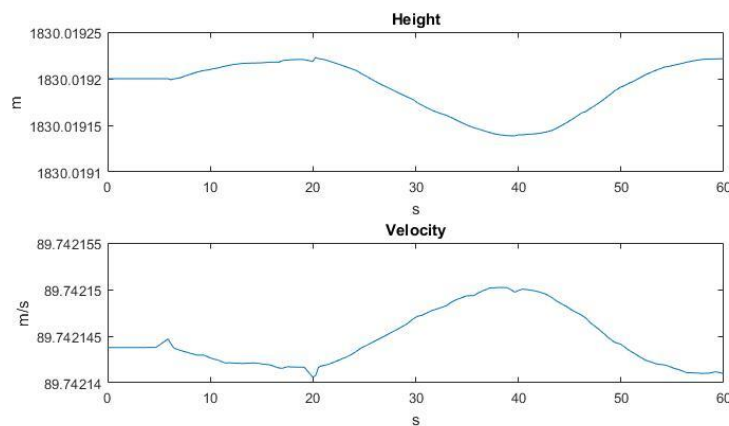


Figure 13: Height and velocity of the simulation of the trimmed aeroplane.

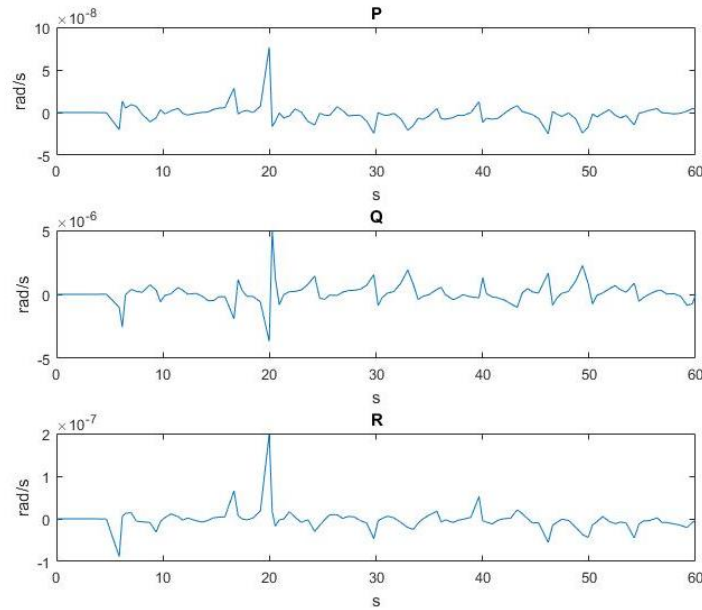


Figure 14: angular velocity of the simulation of the trimmed aeroplane.

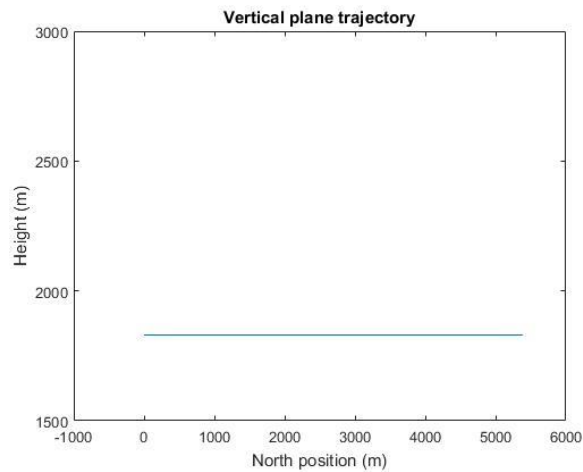


Figure 15: Trajectory over the vertical plane of the simulation of the trimmed aeroplane.

5.4. Non-linear model validation with experimental data

In this section the model will be validated statically with the consolidated flight test data and dynamically with the experimental data of group A in test 2 flight conditions.

5.4.1. Static validation

To validate the non-linear model statically, the flight conditions have been introduced in the consolidated flight test data formulas to obtain the experimental trim conditions. The results for the consolidated

A few assumptions have been made:

- In level flight $C_L \approx C_W$
- The centre of gravity position as a percentage of the mean aerodynamic chord has been computed with the method given in the module Flight Labs:

Table 2: Aeroplane loading and CG calculation.

	mass (kg)	arm (m)	Moment (kg.m)
aircraft including flight crew	4949		27560
seat row 1	0	3.88	0
seat row 2	219	4.64	1016.16
seat row 3	202	5.4	1090.8
seat row 4	172	6.37	1095.64
seat row 5	296	7.13	2110.48
seat row 6	0	7.89	0
CO	80	8.55	684
CA	0	9.55	0
Total	5918		33557.08

fuel (KG)	total mass (kg)	fuel arm (m)	fuel moment (kg.m)	total moment (kg.m)	CG position (%C)
656	6574	5.66	3718.14	37275.22	30.34

With these, the trim values for the control surfaces deflection can be computed and compared to the ones obtained with the model:

Table 3: Comparison of the trim values for the inputs for the consolidated experimental data and the model.

	CONSOLIDATED EXPERIMENTAL DATA	MODEL
ELEVATOR DEFLECTION	-1.234±0.83°	2.240°
AILERON DEFLECTION	2.311°	3.409°
RUDDER DEFLECTION	-0.285°	0°

As it can be seen in Table 3, the differences are noticeable, especially for the elevator deflection which has, in the best case, a 2.644° deviation from the experimental trim data. Furthermore, there is a sign change, which means that while in the tests the aileron was deflected upwards, in the model it is deflected downwards. The error may come from the work the model for the aerodynamic and propulsive effects is based on C.Wolowicz and R. Yancey. Longitudinal aerodynamic characteristics of light, twin-engine, propeller driven airplanes^[3]. Quoting: "...power effects to the calculated pitching-moment characteristics resulted in an increasing disparity between the calculated and the wind-tunnel-derived pitching-moment slopes with increasing power." Even if the power setting was only at about 50% thrust, that may have introduced enough error to account for the elevator trim difference.

Aileron and rudder deflection error in its turn, while still high (a 1.098 and -0.285 degree respectively), do not show this sign change.

5.4.2. Dynamic validation

To validate the non-linear model dynamically, group A in test 2 flight conditions experimental data have been used. The input in the test flights has been introduced to the trimmed model at the given conditions. In order to account for the fact that statically the model trim is off, the input has been modified so that it is relative to the experimental trim value and then it is summed to the model trim value. It must be taken into account that the control surfaces deflection in the experimental files are given in degrees and have to be converted to radians.

In Figure 16 the phugoid response for the model and the experimental data is shown:

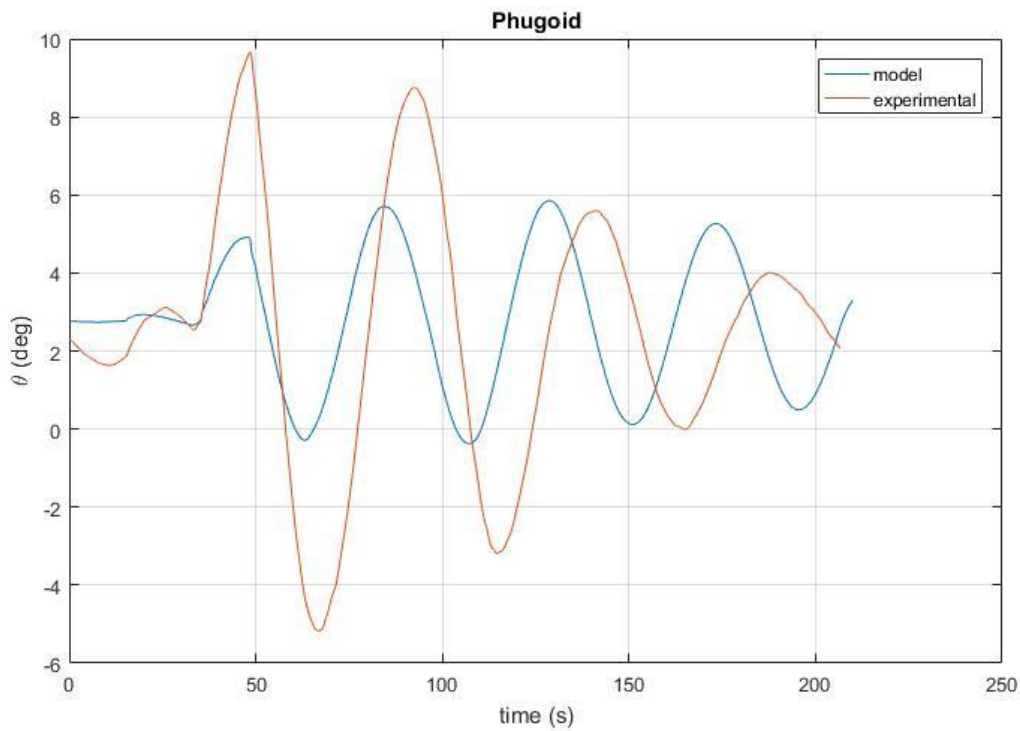


Figure 16: Comparison between model simulation and experimental data- Phugoid mode.

As it can be seen, the initial excitation on the pitch attitude is larger for the experimental data (the peak is a 96.74% larger), although the absolute difference is only about 5 degrees. This difference in amplitude may be due to the approach taken to compare the simulation results versus the experimental data. If instead of shifting the test input to the model trim point, the model trim point was shifted to the real trim point (conserving this way the input as it was in the test), the difference in amplitude may have been lower. Also, the model is based on [3]. In this work it is stated that when different elevator settings other than zero elevator deflection were used, the calculated control effectiveness in pitch differed from the results obtained in wind-tunnel tests.

From the stick release, it can be observed that the frequency of the model is lower than that of the experimental data (0.1417rad/s versus 0.1314rad/s), but the difference is negligible.

Finally, it can be seen that the damping for the model is much lower than the experimental (0.0168 versus 0.0708). This difference may be due to the fact that the aeroplane is considered rigid and does not account for structural dissipation and aeroelastic effects.

In Figure 17 the SPPO response for the model and the experimental data is shown. As it can be seen, the amplitude of the simulation response is overall larger than that of the experimental data. The peak amplitude of the simulation is a 47.59% higher than that of the experimental data, although, again, the absolute difference is only of 5 deg/s. The reasons for this difference are analogous to that of the phugoid.

The damping ratio of the model is slightly lower (0.4687 for the simulation versus 0.4994 for the experimental data) but the difference is overall negligible.

In this case, the frequency of the model is notably higher in the simulation (4.69rad/s for the simulation versus 2.61rad/s for the experimental data). Again, this may be due to the fact that the aeroplane is considered rigid.

It can also be noted that the simulation has a slight lag compared to the experimental data of about 0.1 seconds. This difference is due to the fact that the model does not simulate the actuators, which leads to a faster response.

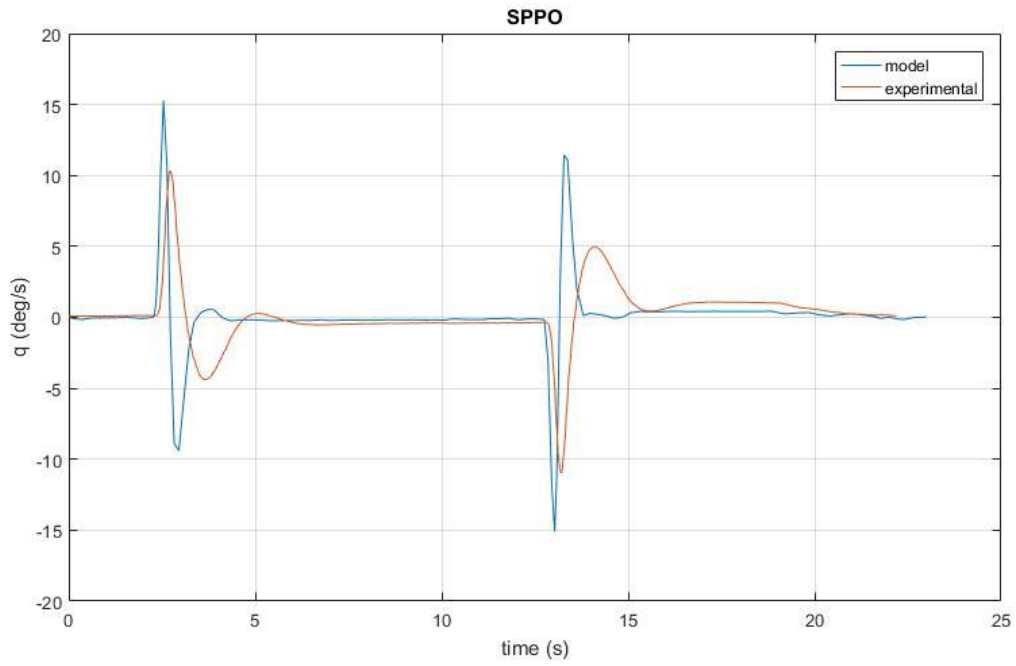


Figure 17: Comparison between model simulation and experimental data- SPPO mode.

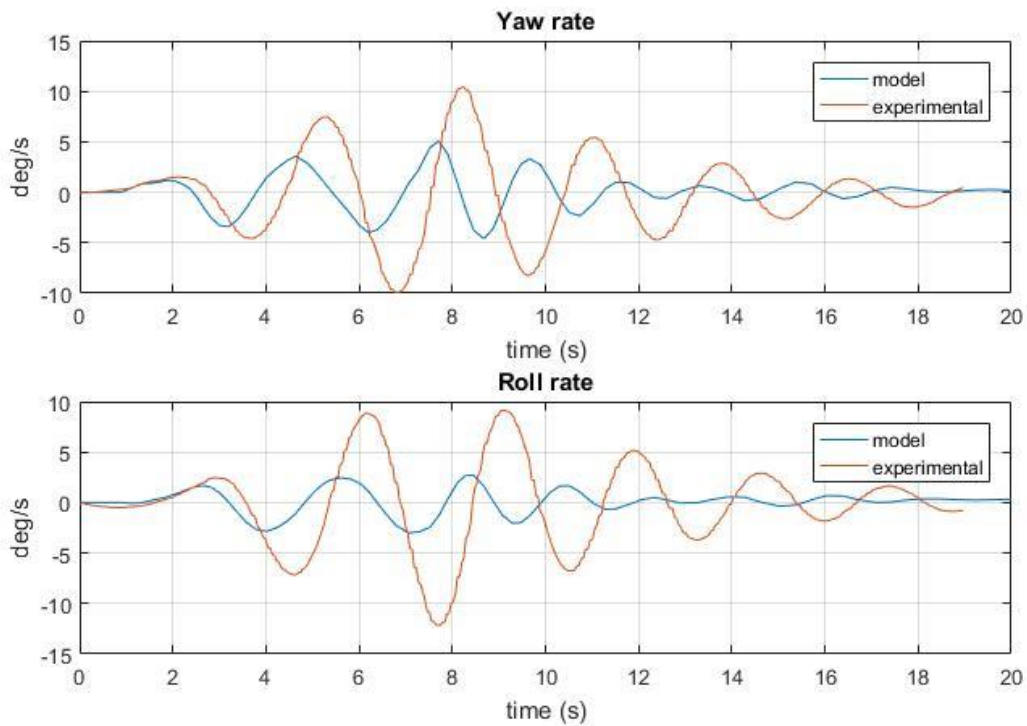


Figure 18: Comparison between model simulation and experimental data- Dutch roll.

In Figure 18 the dutch roll response for the model and the experimental data is shown. It can be observed that the experimental data shows a greater dutch roll excitation than the model, with a peak amplitude difference of a 108.4% and a 69.9% in yaw rate and roll rate respectively, although similarly to the previous analysis, the absolute difference is about 5 degrees. The reason for these differences may be due to the aerodynamic and propulsive module, which for lateral-directional effects was based on C.Wolowicz and R. Yancey. Lateral-directional aerodynamic characteristics of light, twin-engine, propeller driven ^{airplanes[4]}. In this document, it is stated that “The calculated roll-to-sideslip amplitude ratio of the dutch roll mode did not correlate well with flight data”, which may explain the difference in amplitude, together with the fact that the model does not account for non-rigid aeroplane body.

In this case, the frequencies are fairly similar, with a yaw rate frequency of 2.127rad/s for the experimental data and 1.972rad/s for the simulation and a roll rate frequency of 2.004rad/s for the experimental data and 2.063rad/s for the simulation. The differences may be explained quoting [4] “The calculated dutch roll period was generally 10% lower than the flight values”.

The damping ratio is lower for the simulation, although for the roll rate the values are fairly similar (yaw rate damping of 0.1038 for the experimental data and 0.0674 for the simulation and a roll rate damping of 0.0884 for the experimental data and 0.0767 for the simulation).

Finally, the roll mode response can be found in Figure 19. As it can be seen, the model has a more excited response, with a peak amplitude of 102.7 deg in the simulation compared to the 33.02 deg of the experimental data and an undershoot of -92.85 deg compared to the .28.96 deg of the experimental data. The error here may be similar to the amplitude error in the phugoid mode. If instead of shifting the input to the model’s trim point, the model’s trim point was shifted to the experimental trim point (conserving the input as it is), the simulation would have been more accurate.

It can also be noted that the response is slightly delayed, being the model response about 0.8 seconds earlier. This delay may be explained as the model did not account for the actuators dynamic response, which generally introduce a delay.

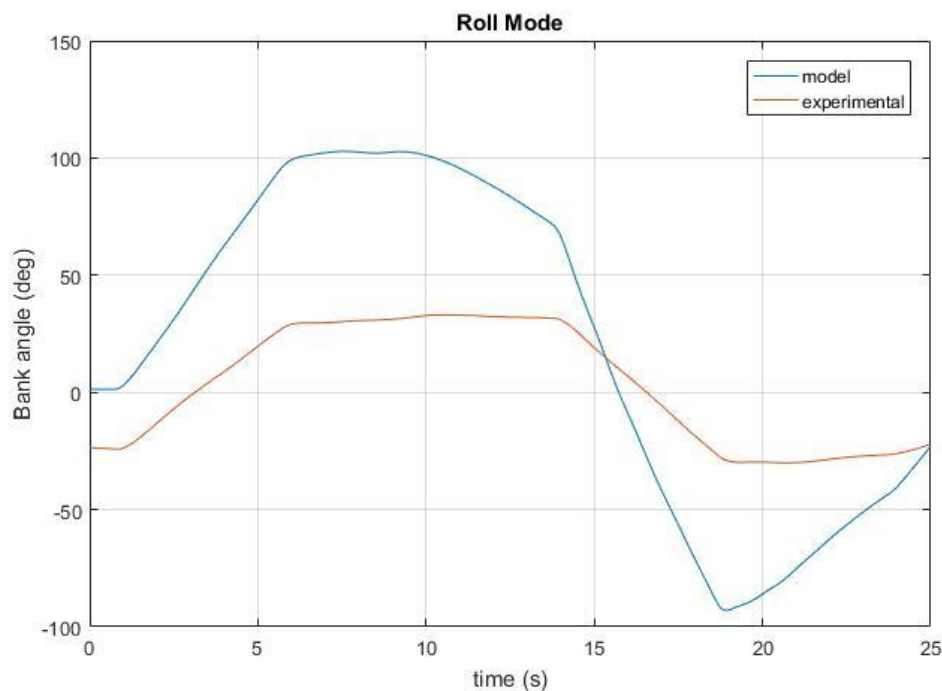


Figure 19: Comparison between model simulation and experimental data- Roll mode.

6. Lineal model

In this section, the model is linearized which enables it to be decoupled.

6.1. Construction of the lineal model

The linearization is carried out with the Matlab® function 'linmod' around the trim state found in the previous section. The output state space matrices are:

$$A = \begin{bmatrix} -0.0141 & 0 & 0.1606 & -0.0016 & -3.1675 & 2.3072 & 0 & -9.7992 & 0 & 0 & 0 & 0 \\ 0 & -0.1991 & 0 & 4.2808 & 0 & -88.9995 & 9.7961 & -0.0107 & 0 & 0 & 0 & 0 \\ -0.1707 & -0.0053 & -1.0816 & -2.2842 & 86.7859 & -0.0026 & -0.2212 & -0.4688 & 0 & 0 & 0 & -0.0022 \\ 0 & -0.0682 & 0.0027 & -2.1364 & 0.0031 & 0.8127 & 0 & 0 & 0 & 0 & 0 & 0 \\ 0.0134 & -0.0034 & -0.3402 & -0.0045 & -7.2786 & -0.0085 & 0.0022 & 0.0047 & 0 & 0 & 0 & 0 \\ -0.003 & 0.0992 & 0.0039 & -1.0012 & -0.0099 & -0.7869 & 0 & 0 & 0 & 0 & 0 & 0 \\ 0 & 0 & 0 & 1 & 0.0011 & 0.0482 & 0 & 0 & 0 & 0 & 0 & 0 \\ 0 & 0 & 0 & 0 & 0.9997 & -0.0227 & 0 & 0 & 0 & 0 & 0 & 0 \\ 0 & 0 & 0 & 0 & 0.0228 & 1.0009 & 0 & 0 & 0 & 0 & 0 & 0 \\ 0.9985 & 0.0257 & 0.0475 & 0 & 0 & 0 & 0 & 0 & 0 & 0 & 0 & 0 \\ -0.0246 & 0.9994 & -0.0239 & 0 & 0 & 0 & -4.3190 & 0 & 89.7421 & 0 & 0 & 0 \\ -0.0481 & 0.0227 & 0.9986 & 0 & 0 & 0 & 2.2089 & -89.7149 & 0 & 0 & 0 & 0 \end{bmatrix}$$

$$B = \begin{bmatrix} 3.5878 & -0.0746 & 0.1807 & 0.0336 \\ 0.002 & 3.7374 & 0.5528 & 0 \\ -15.7793 & -0.0084 & 0.0557 & 0.0013 \\ 0.0114 & 1.3537 & -16.4871 & 0.0044 \\ -26.1554 & 0.0194 & -0.0065 & 0.0088 \\ 0.002 & -4.2392 & 51.2251 & 0 \\ 0 & 0 & 0 & 0 \\ 0 & 0 & 0 & 0 \\ 0 & 0 & 0 & 0 \\ 0 & 0 & 0 & 0 \\ 0 & 0 & 0 & 0 \\ 0 & 0 & 0 & 0 \end{bmatrix}$$

Where the obvious residuals have been replaced by 0. Now, the matrices can be decoupled into longitudinal mode and lateral-directional, where the state space variables and input vectors will be:

$$x_{long} = [u \ w \ q \ \theta] \quad u_{long} = [\eta \ \tau] \quad x_{lat} = [v \ p \ r \ \phi \ \psi] \quad u_{lat} = [\zeta \ \xi]$$

Leading to the following state space matrices:

$$A_{long} = \begin{bmatrix} -0.0141 & 0.1606 & -3.1675 & -9.7992 \\ -0.1707 & -1.0816 & 86.7859 & -0.4688 \\ 0.0134 & -0.3402 & -7.2786 & 0.0047 \\ 0 & 0 & 0.9997 & 0 \end{bmatrix}$$

$$B_{long} = \begin{bmatrix} 3.5878 & 0.0336 \\ -15.7793 & 0.0013 \\ -26.1554 & 0.0088 \\ 0 & 0 \end{bmatrix}$$

$$A_{lat} = \begin{bmatrix} -0.1991 & 4.2808 & -88.9995 & 9.7961 & 0 \\ -0.0682 & -2.1364 & 0.8127 & 0 & 0 \\ 0.0992 & -1.0012 & -0.7869 & 0 & 0 \\ 0 & 1 & 0.0482 & 0 & 0 \\ 0 & 0 & 1.0009 & 0 & 0 \end{bmatrix}$$

$$B_{lat} = \begin{bmatrix} 3.7374 & 0.5528 \\ 1.3537 & -16.4871 \\ -4.2392 & 51.2251 \\ 0 & 0 \\ 0 & 0 \end{bmatrix}$$

And where C and D matrices will be the identity and zeros in both cases. From these state space representations the transfer functions can be obtained:

$$\begin{aligned}\frac{u}{\eta} &= \frac{3.5878(s + 30.07)(s^2 + 0.6729s + 2.094)}{(s^2 + 0.01547s + 0.01895)(s^2 + 8.359s + 37.43)} \left[\frac{m}{s \cdot rad} \right] \\ \frac{w}{\eta} &= \frac{-15.779(s + 151.2)(s^2 + 0.01516s + 0.01914)}{(s^2 + 0.01547s + 0.01895)(s^2 + 8.359s + 37.43)} \left[\frac{m}{s \cdot rad} \right] \\ \frac{q}{\eta} &= \frac{-26.155s(s + 0.8522)(s + 0.03653)}{(s^2 + 0.01547s + 0.01895)(s^2 + 8.359s + 37.43)} \left[\frac{1}{s} \right] \\ \frac{\theta}{\eta} &= \frac{-26.149(s + 0.8522)(s + 0.03653)}{(s^2 + 0.01547s + 0.01895)(s^2 + 8.359s + 37.43)}\end{aligned}$$

$$\begin{aligned}\frac{u}{\tau} &= \frac{0.03357(s - 0.07447)(s^2 + 7.606s + 38.24)}{(s^2 + 0.01547s + 0.01895)(s^2 + 8.359s + 37.43)} \left[\frac{m}{s} \right] \\ \frac{w}{\tau} &= \frac{0.0013116(s + 588.5)(s^2 + 0.01155s + 0.01908)}{(s^2 + 0.01547s + 0.01895)(s^2 + 8.359s + 37.43)} \left[\frac{m}{s} \right] \\ \frac{q}{\tau} &= \frac{0.0088492s(s^2 + 1.096s + 0.3175)}{(s^2 + 0.01547s + 0.01895)(s^2 + 8.359s + 37.43)} \left[\frac{rad}{s} \right] \\ \frac{\theta}{\tau} &= \frac{0.0088469(s^2 + 1.096s + 0.3175)}{(s^2 + 0.01547s + 0.01895)(s^2 + 8.359s + 37.43)} [rad]\end{aligned}$$

$$\begin{aligned}\frac{v}{\zeta} &= \frac{3.7374s(s + 103)(s + 2.465)(s - 0.02975)}{s(s + 2.467)(s - 0.01516)(s^2 + 0.6704s + 10.59)} \left[\frac{m}{s \cdot rad} \right] \\ \frac{p}{\zeta} &= \frac{1.3537s(s - 4.222)(s + 2.48)(s - 0.005158)}{s(s + 2.467)(s - 0.01516)(s^2 + 0.6704s + 10.59)} \left[\frac{1}{s} \right] \\ \frac{r}{\zeta} &= \frac{-4.2392s(s + 2.465)(s^2 + 0.1027s + 0.1452)}{s(s + 2.467)(s - 0.01516)(s^2 + 0.6704s + 10.59)} \left[\frac{1}{s} \right] \\ \frac{\phi}{\zeta} &= \frac{1.1495s(s - 4.994)(s + 2.48)}{s(s + 2.467)(s - 0.01516)(s^2 + 0.6704s + 10.59)} \\ \frac{\psi}{\zeta} &= \frac{-4.243(s + 2.465)(s^2 + 0.1027s + 0.1452)}{s(s + 2.467)(s - 0.01516)(s^2 + 0.6704s + 10.59)}\end{aligned}$$

$$\begin{aligned}\frac{v}{\xi} &= \frac{0.55285s(s - 8374)(s + 2.454)(s - 0.02994)}{s(s + 2.467)(s - 0.01516)(s^2 + 0.6704s + 10.59)} \left[\frac{m}{s \cdot rad} \right] \\ \frac{p}{\xi} &= \frac{-16.487s(s - 4.079)(s + 2.547)(s - 0.005121)}{s(s + 2.467)(s - 0.01516)(s^2 + 0.6704s + 10.59)} \left[\frac{1}{s} \right] \\ \frac{r}{\xi} &= \frac{51.225s(s + 2.454)(s^2 + 0.2049s + 0.1449)}{s(s + 2.467)(s - 0.01516)(s^2 + 0.6704s + 10.59)} \left[\frac{1}{s} \right] \\ \frac{\phi}{\xi} &= \frac{-14.02s(s - 4.828)(s + 2.552)}{s(s + 2.467)(s - 0.01516)(s^2 + 0.6704s + 10.59)} \\ \frac{\psi}{\xi} &= \frac{51.271(s + 2.454)(s^2 + 0.2049s + 0.1449)}{s(s + 2.467)(s - 0.01516)(s^2 + 0.6704s + 10.59)}\end{aligned}$$

6.2. Validation against the non-linear model

In this section the linearized model response is compared with the non-linear model to validate its response. The inputs have been set up so that they are the same for both the non-linear model and the linearized model.

In Figure 20, the forward velocity has been plotted for the phugoid mode for both models. As it can be seen, initially the signals are very close, only with a slight deviation in amplitude and rise time (the first peak of the linearized model is a 0.002% higher, given 0.56 seconds later). The damping ratio for both models is identical ($3.5498e-0.5$). It can also be observed that the frequency is slightly lower for the linearized model (0.1381rad/s for the linear model compared to 0.1385rad/s for the non-linear model). Overall it can be said that the tracking of the linear model with the non-linear model is good, although the difference in frequency, even if small, will affect the long term outputs significantly.

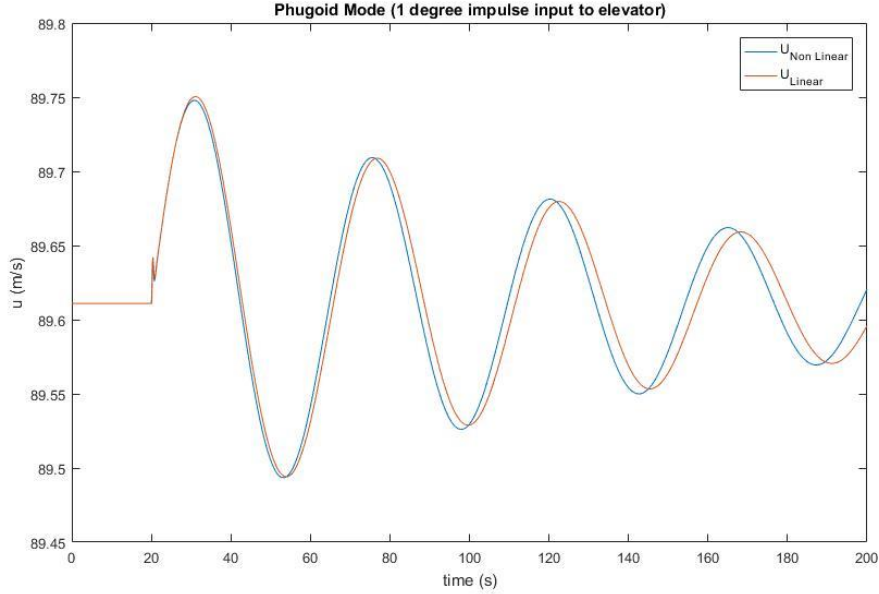


Figure 20: Comparison between the non-linear and linear model – Phugoid mode.

In Figure 21, the SPPO response for the two models is shown. Similarly to the phugoid mode, the tracking of the linearized model is good. The peak amplitude of the first peak of the linearized model is slightly smaller (a 1.02% smaller) and it can be seen that the settling time is lower (about 0.1 seconds). Overall, the differences are negligible.

In Figure 22, the dutch roll response is shown. As it can be observed, the linearized response fits almost perfectly the non-linear model and the differences in signals are smaller than the precision of the results given by the simulation of the non-linear model, so it can be considered that it is a perfect fit.

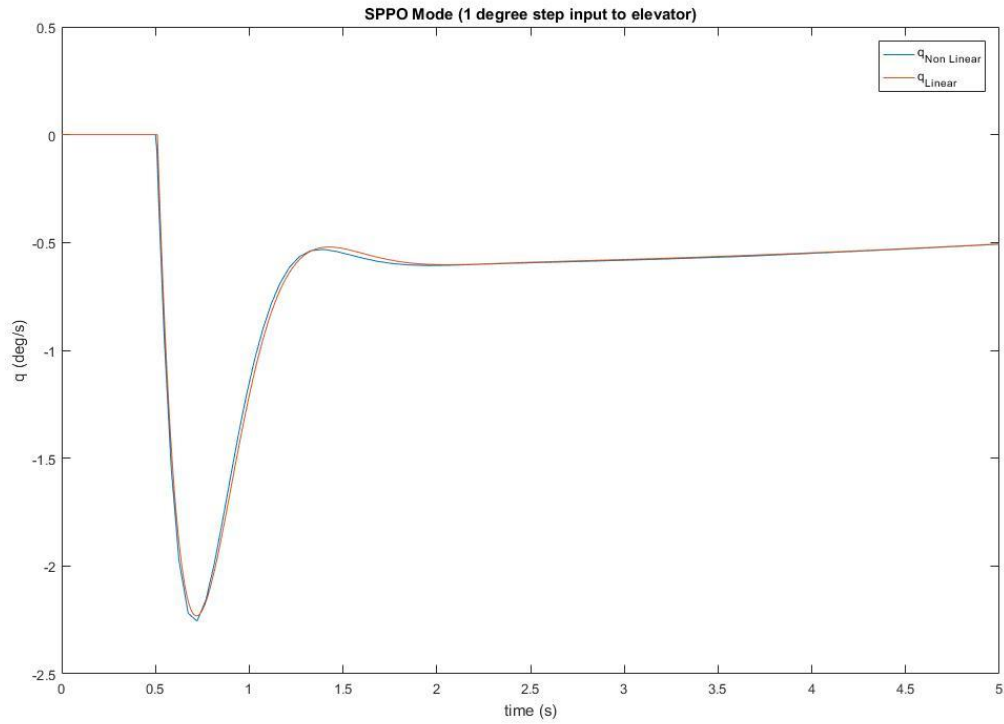


Figure 21: Comparison between the non-linear and linear model – SPPO mode.

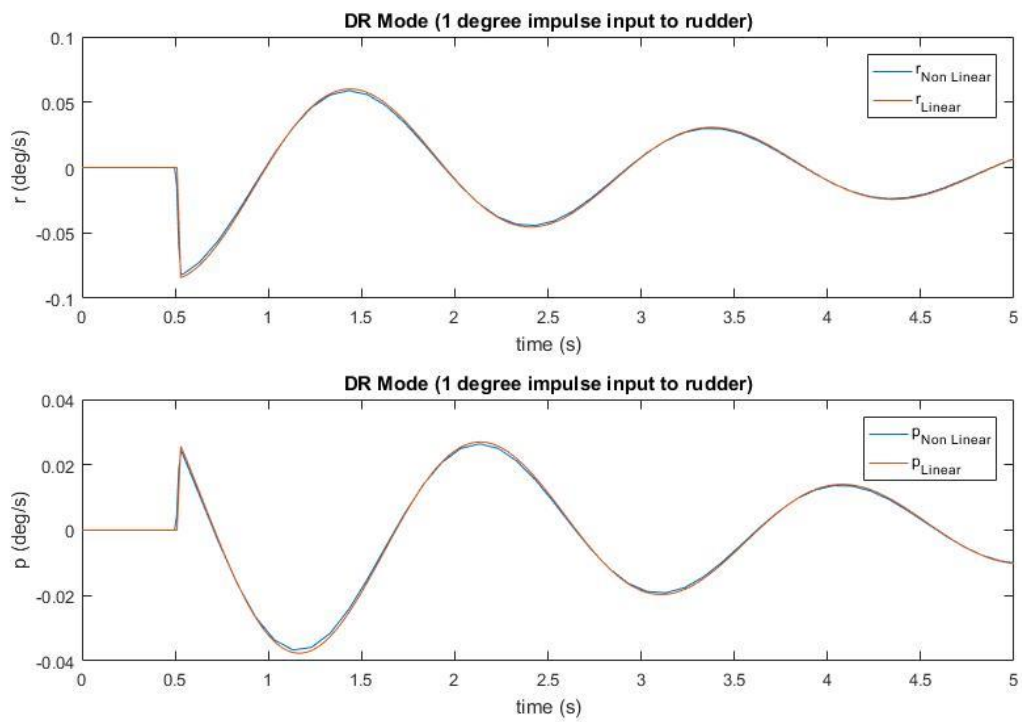


Figure 22: Comparison between the non-linear and linear model – Dutch roll mode.

In Figure 23, the roll mode response for the non-linear and the linear models have been plotted. As it can be seen, both responses are almost identical, being the difference between them smaller than the precision required to the non-linear model solver.

Finally, in Figure 24, the spiral mode is shown. The response diverges slightly, being the rolling angular acceleration slightly smaller for the linear model, but the difference will not be relevant for simulation times lower than 100 seconds.

Overall the linearized model fits well with the non-linear model, except for a slight difference in amplitude and frequency in the phugoid mode and in the rolling angular acceleration of the spiral mode which may only create problems in long time simulations.

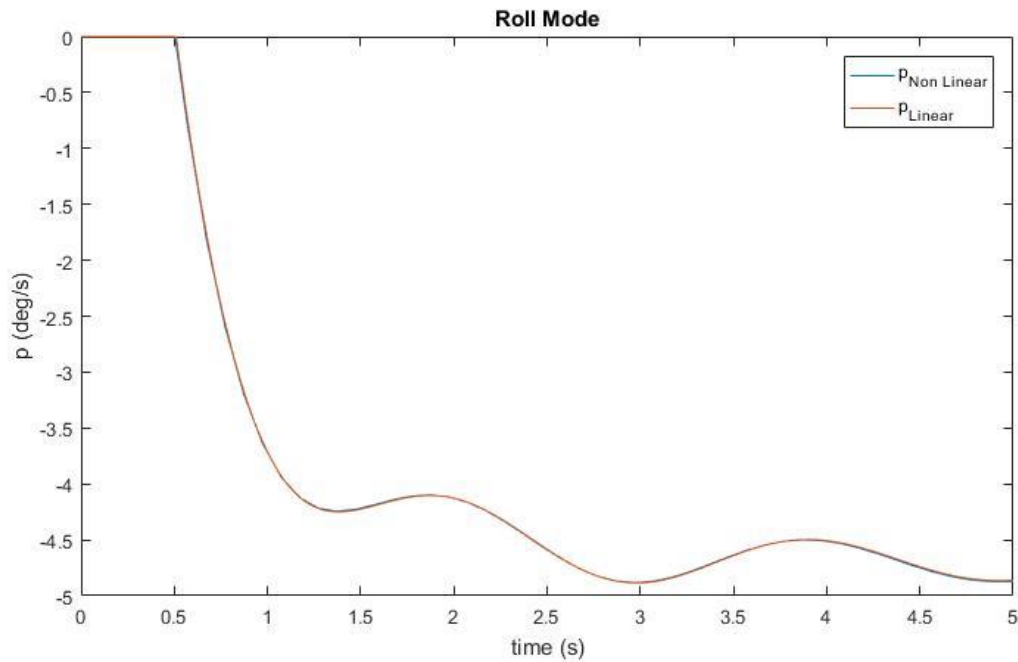


Figure 23: Comparison between the non-linear and linear model – Roll mode.

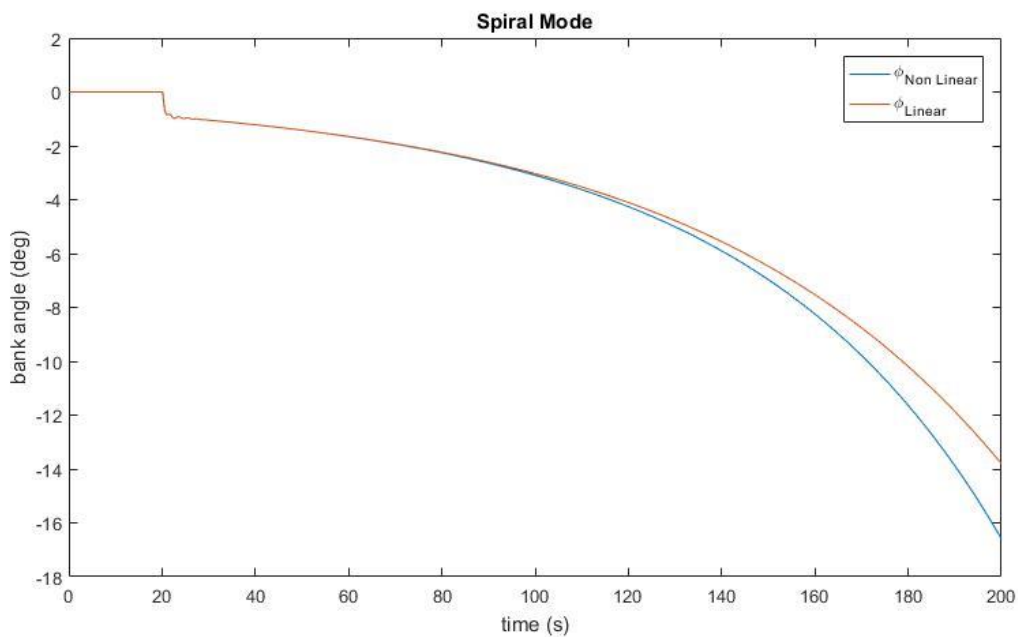


Figure 24: Comparison between the non-linear and linear model – Spiral mode.

7. Frequency domain analysis

The handling qualities of the aircraft can be predicted from the frequency domain analysis. The pitch tracking task is generally regarded as one of the most critical aspects of longitudinal handling, hence the transfer function under study will be pitch to elevator. Firstly, the transfer function has been modified in order to include a time delay of 0.01s that accounts for the mechanical 'slop' and backlash:

$$\frac{\theta}{\eta} = \frac{-26.149(s + 0.8522)(s + 0.03653)e^{-0.01s}}{(s^2 + 0.01547s + 0.01895)(s^2 + 8.359s + 37.43)}$$

Now the bode plot can be obtained (see Figure 25).

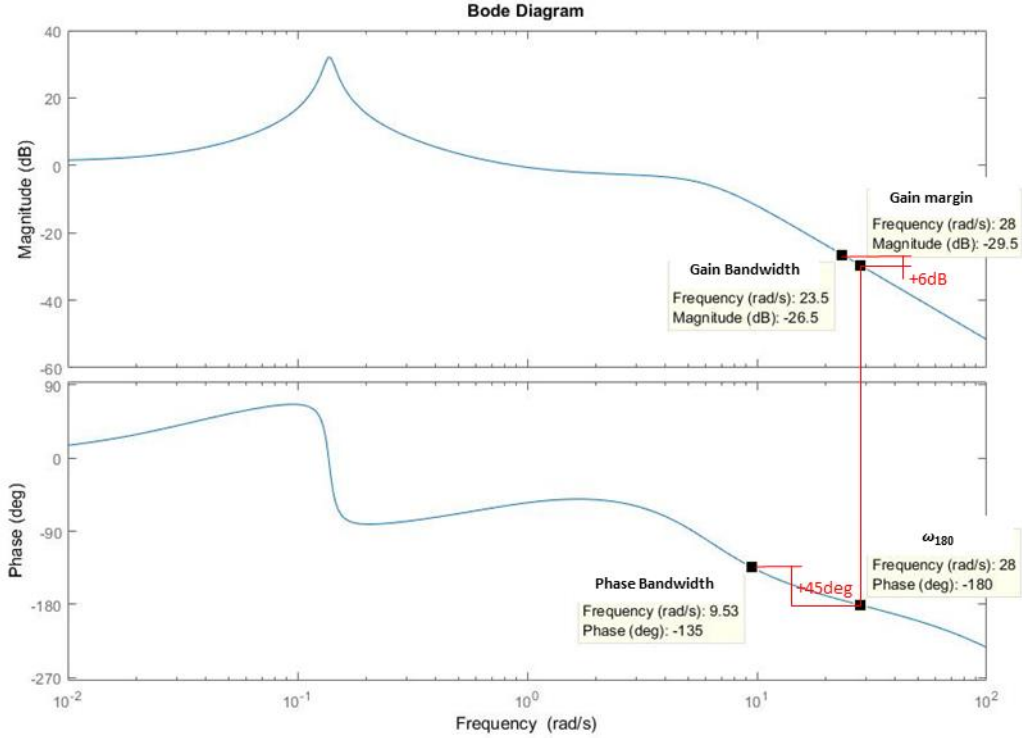


Figure 25: Bode plot of the pitch to elevator transfer function.

In order to assess the handling qualities, two parameters have to be defined:

- Phase bandwidth: frequency at which the phase margin is 45deg: $\omega_{BW_{phase}} = 9.53 \text{ rad/s}$
- Gain bandwidth: frequency at which the gain margin is 6dB: $\omega_{BW_{gain}} = 23.5 \text{ rad/s}$
- Phase delay: the value of the phase roll-off at ω_{180} in seconds: $\tau_p = \frac{10}{\omega_{180} - \omega_{175}} \cdot \frac{\pi}{180} = 0.0388 \text{ s}$

The bandwidth is defined as the lower of the two, in this case $\omega_{BW} = 9.53 \text{ rad/s}$, and since this is the phase bandwidth the system is said to be phase margin limited.

The criterion to check the handling qualities is based on testing and is expressed graphically as boundaries of equivalent phase delay as a function of pitch attitude bandwidth. The boundaries defined in MIL-STD-1797A for category A, together with the point corresponding to the data obtained, is shown in Figure 26. As it can be seen, the model of the airplane is compliant with level 1 requirements, hence it is expected that it will have good handling qualities.

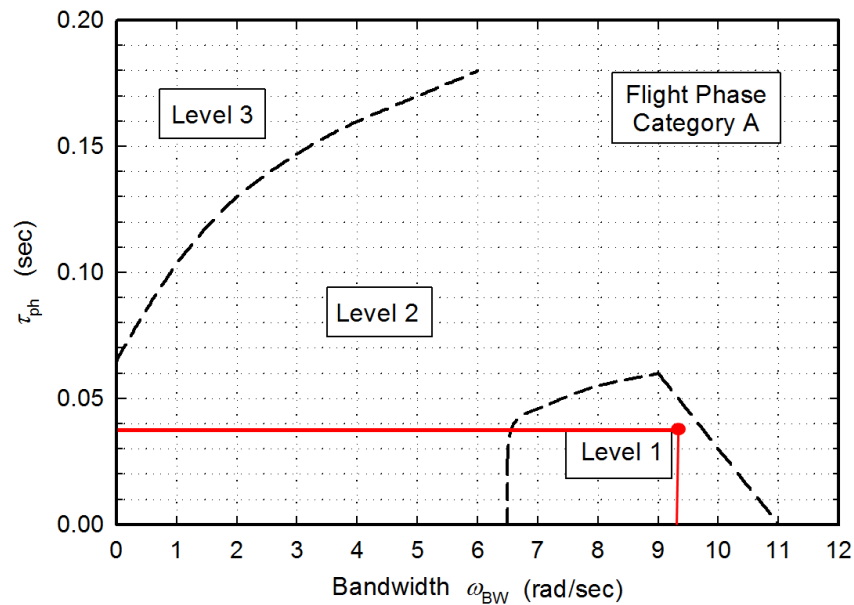


Figure 26: Pitch attitude bandwidth requirement for flight phase category A. From MIL-STD-1797A.

8. Conclusions

8.1. Equations of motion sub-model

A sub-model which solves the equations of motion through euler angles has been developed. A sub-model which computes the forces and moments applied on the BAC by the weight due to the fact that the CG is not centered in the BAC has also been developed. The model has been verified through 5 tests:

- Isolated initial conditions: without forces or moments applied, the model should conserve the initial conditions introduced. The model response was as expected.
- Isolated unitary forces: applying unitary forces with zero initial conditions and moments, the model had to show a uniformly accelerated longitudinal movement. The model response was as expected.
- Isolated unitary moments: applying independent unitary moments with zero initial conditions and forces, the model had to show a uniformly accelerated angular movement. The model response was as expected.
- Free fall test: with the gravity forces and moments module connected, with no other forces or moments applied and with initial conditions equal to zero except for the altitude, set to 1000m, the model had to show a free fall movement where the fall time was 20.20 seconds and the attitude was maintained. The model response was as expected.
- Pendulum test: with only the moments of the gravity forces and moments module connected and with an initial attitude of $-\pi/4$ rad in bank angle and the CG located at 1m along the y-axis, the model had to display a pendular motion in bank angle with a period equal to that of a pendulum of 1m of string. The model response was as expected.

8.2. Model assembly and trim

A model of the Jetstream 31 was assembled. The sub-models used were the Equations of motion sub-model and the gravity forces and moments developed previously, a sub-model which computes from the output of the equations of motion the flight conditions, and a sub-model provided by Cranfield University which computes the aerodynamic and propulsive forces and moments of the Jetstream 31 given its flight conditions. The model was trimmed at the following state:

- Passenger and crew loading matrix:

$$\begin{bmatrix} 86 & 0 & 69 & 65 & 64 & 86 & 0 & 180 \\ 86 & 0 & 75 & 68 & 58 & 90 & 0 & 80 \\ 0 & 0 & 75 & 69 & 50 & 120 & 0 & 0 \end{bmatrix} Kg$$

- Fuel: 656 Kg
- Flap: retracted (0)
- Undercarriage: up (0)
- Altitude: 6004 ft
- EAS: 161 kts

Which is the flight conditions given in the flight tests of Group A, test configuration 2. These led to the following trim state:

- State space variables:
 - $\begin{bmatrix} u \\ v \\ w \end{bmatrix} = \begin{bmatrix} 89.6 \\ 2.3 \\ 4.3 \end{bmatrix} m/s$
 - $\begin{bmatrix} p \\ q \\ r \end{bmatrix} = \begin{bmatrix} 0 \\ 0 \\ 0 \end{bmatrix} rad/s$
 - $\begin{bmatrix} \phi \\ \theta \\ \psi \end{bmatrix} = \begin{bmatrix} 0.052 \\ 0.158 \\ -0.109 \end{bmatrix} rad$
 - $\begin{bmatrix} North \\ East \\ Down \end{bmatrix} = \begin{bmatrix} 0 \\ 0 \\ -1830 \end{bmatrix} m$
- Outputs
 - $V = 89.7421 m/s$
 - $\alpha_b = 0.0476 rad$
 - $\beta_b = 0.0257 rad$
- Inputs
 - $\eta = 0.0391 rad$
 - $\zeta = 0.0595 rad$
 - $\xi = 0 rad$
 - $\tau = 51.35\%$

8.3. Model verification

The model was verified statically and dynamically with experimental data. Statically, the model was verified with consolidated flight data, the results of which can be seen in Table 4:

Table 4: Static trim values comparison.

	CONSOLIDATED EXPERIMENTAL DATA	MODEL
ELEVATOR DEFLECTION	-1.234±0.83°	2.240°
AILERON DEFLECTION	2.311°	3.409°
RUDDER DEFLECTION	-0.285°	0°

As it can be seen, the differences are noticeable, especially for the elevator deflection which has, in the best case, a 2.644° deviation from the experimental trim data. Furthermore, there is a sign change, which means that while in the tests the aileron was deflected upwards, in the model it is deflected downwards. The error may come from the work the model for the aerodynamic and propulsive effects is based on [3]. Quoting: "...power effects to the calculated pitching-moment characteristics resulted in an increasing disparity between the calculated and the wind-tunnel-derived pitching-moment slopes with increasing power.". Even if the power setting was only at about 50% thrust, that may have introduced enough error to account for the elevator trim difference.

Aileron and rudder deflection error in its turn, while still high (a 1.098 and -0.285 degree respectively), do not show this sign change.

The model was verified dynamically with the experimental data of the flight tests of Group A, test configuration 2. Below, a table comparing the results of the simulation and the experimental data is shown (Table 5):

Table 5: Summary of the results of the comparison between the simulation response and the experimental data.

	Phugoid		SPPO		Dutch Roll			Roll Mode	
	Model	Experimental	Model	Experimental	Model	Experimental		Model	Experimental
Peak amplitude	4.916 deg	9.662 deg	15.29 deg/s	10.36 deg/s	Yaw rate	5.082 deg/s	10.41 deg/s	102.7 deg	33.02 deg
					Roll rate	2.682 deg/s	9.113 deg/s		
Frequency (rad/s)	0.1417	0.1314	4.69	2.61	Yaw rate	1.972	2.127	-	-
					Roll rate	2.063	2.004	-	-
Damping	0.0168	0.0708	0.4687	0.4994	Yaw rate	0.0674	0.1038	-	-
					Roll rate	0.0767	0.0884	-	-

In addition to these results, it may also be added that there was a delay in the experimental data with respect to the simulation data of 0.1 and 0.08 seconds for the SPPO and the roll mode respectively

The amplitude difference in the phugoid mode may be due to the approach taken to compare the simulation results versus the experimental data. The input of the experimental data was shifted from the experimental trim point to the simulation trim point. If instead, the model trim point was shifted to the experimental data trim point, maintaining the input as in the experiments, the difference in amplitude may have been lower. Also, the model is based on [3]. In this work it is stated that when different elevator settings other than zero elevator deflection were used, the calculated control effectiveness in pitch differed from the results obtained in wind-tunnel tests, which could influence the amplitude of this mode.

The frequency of the model for the phugoid mode was lower than that of the experimental data, but the difference is negligible. The damping for the model was much lower than the experimental. This difference may be due to the fact that the aeroplane is considered rigid and does not account for structural dissipation and aeroelastics effects.

For the SPPO, the amplitude of the simulation response was overall larger than that of the experimental data. The reasons for this difference are analogous to that of the phugoid. The damping ratio of the model for the SPPO was slightly lower, but the difference is overall negligible. In this case, the frequency of the model was notably higher in the simulation. Again, this may be due to the fact that the aeroplane is considered rigid. The lag of the experimental data with the simulation data may be due to the fact that the model does not simulate the actuators, which leads to a faster response.

For the dutch roll, it can be observed that the experimental data shows a greater excitation. The reason for these differences may be due to the aerodynamic and propulsive module, which for lateral-directional effects was based on [4]. In this document, it is stated that “The calculated roll-to-sideslip amplitude ratio of the dutch roll mode did not correlate well with flight data”, which may explain the difference in amplitude, together with the fact that the model does not account for non-rigid aeroplane body.

The frequencies of the dutch roll were fairly similar. The differences may be explained quoting [4] “The calculated dutch roll period was generally 10% lower than the flight values”. The damping ratio was lower for the simulation, although for the roll rate the values were fairly. Overall the differences were negligible.

For the roll mode, the model had a more excited response. The error here may be similar to the amplitude error in the phugoid mode: if instead of shifting the input to the model’s trim point, the model’s trim point was shifted to the experimental trim point (conserving the input as it is), the simulation would have been more accurate. The delay in the roll mode may be explained as the model did not account for the actuators dynamic response, which generally introduce a delay, thus making the simulation faster than the experimental data.

Overall the model response was acceptable, although design and testing should be approached with care taking into account its limitations and deficiencies.

8.4. Linearized model and validation against the non-linear model

The model was linearized around the trim point and decoupled in longitudinal and lateral-directional models. The resulting state space matrices were:

$$A_{long} = \begin{bmatrix} -0.0141 & 0.1606 & -3.1675 & -9.7992 \\ -0.1707 & -1.0816 & 86.7859 & -0.4688 \\ 0.0134 & -0.3402 & -7.2786 & 0.0047 \\ 0 & 0 & 0.9997 & 0 \end{bmatrix}$$

$$B_{long} = \begin{bmatrix} 3.5878 & 0.0336 \\ -15.7793 & 0.0013 \\ -26.1554 & 0.0088 \\ 0 & 0 \end{bmatrix}$$

$$A_{lat} = \begin{bmatrix} -0.1991 & 4.2808 & -88.9995 & 9.7961 & 0 \\ -0.0682 & -2.1364 & 0.8127 & 0 & 0 \\ 0.0992 & -1.0012 & -0.7869 & 0 & 0 \\ 0 & 1 & 0.0482 & 0 & 0 \\ 0 & 0 & 1.0009 & 0 & 0 \end{bmatrix}$$

$$B_{lat} = \begin{bmatrix} 3.7374 & 0.5528 \\ 1.3537 & -16.4871 \\ -4.2392 & 51.2251 \\ 0 & 0 \\ 0 & 0 \end{bmatrix}$$

The linear model response was compared to the non-linear model response for all the modes. The dutch roll and roll mode responses had a perfect fit. The SPPO mode showed a slightly smaller peak amplitude in the linearized response (1.02% smaller to that of the non-linear model) and frequency (0.1381rad/s compared to 0.1385rad/s), but overall the differences were negligible.

For the phugoid mode, initially the signals were very close, only with a slight deviation in amplitude and rise time (the first peak of the linearized model is a 0.002% higher, given 0.56 seconds later). The damping ratio for both models was identical (3.5498e-0.5) and the frequency was slightly lower for the linearized model (0.1381rad/s for the linear model compared to 0.1385rad/s for the non-linear model). Overall, the tracking of the linear model with the non-linear model was good, although the difference in frequency, even if small, would affect long term simulations outputs significantly.

Finally, for the spiral mode, the response diverged slightly, being the rolling angular acceleration slightly smaller for the linear model, but the difference would not be relevant for simulation times lower than 100 seconds.

Overall the linearized model fits well with the non-linear model, except for a slight difference in amplitude and frequency in the phugoid mode and in the rolling angular acceleration of the spiral mode which may only create problems in long time simulations.

8.5. Frequency domain analysis

A frequency domain analysis was carried out using the linearized model. The task analysed was the pitch tracking task, at it is considered a critical one regarding the handling qualities of the aeroplane. The results obtained were:

- Phase bandwidth: $\omega_{BW_{phase}} = 9.53 \text{ rad/s}$
- Gain bandwidth: $\omega_{BW_{gain}} = 23.5 \text{ rad/s}$
- Phase delay: $\tau_P = \frac{10}{\omega_{180} - \omega_{175}} \cdot \frac{\pi}{180} = 0.0388 \text{ s}$

Giving a bandwidth of $\omega_{BW} = 9.53 \text{ rad/s}$ (hence the system is phase margin limited).

The model of the airplane is compliant with level 1 requirements of the in MIL-STD-1797A for category A, hence it is expected that it will have good handling qualities. Since the difference in frequency of the model compared to the experimental data is acceptable, it can be deduced that the real aeroplane will be also be compliant.

9. References

- [1] A. Cooke, Dynamic Stability and Modal Analysis, Cranfield University, 2016
- [2] A. Cooke, Flight Dynamic Principles: Data Pack for the Jetstream 31, Cranfield University, 2016
- [3] C.Wolowicz and R. Yancey. Longitudinal aerodynamic characteristics of light, twin-engine, propeller driven airplanes. Technical Report NASA TN D-6800, National Aeronautics and Space Administration, June 1972
- [4] C.Wolowicz and R. Yancey. Lateral-directional aerodynamic characteristics of light, twin-engine, propeller driven airplanes. Technical Report NASA TN D-6946, National Aeronautics and Space Administration, October 1972.